Journal of Fluorescence (2019) 29:435–443
https://doi.org/10.1007/s10895-019-02352-w

ORIGINAL ARTICLE

Photoluminescence Properties of Dy^{3+} Activated $CaWO_4$ Nanophosphors: a Potential Single Phase near White Light Emitter

Takhe Yaba[1] · Ranjoy Wangkhem[1] · N. Shanta Singh[1]

Received: 29 November 2018 / Accepted: 14 January 2019 / Published online: 26 January 2019

Abstract

A multicolor tunable $CaWO_4:xDy^{3+}$ nanophosphors have been synthesized via hydrothermal route. X-Ray Diffraction and Fourier transform infrared confirm the formation of $CaWO_4:Dy^{3+}$ nanophosphors. Transmission electron microscopy image and selected area electron diffraction (SAED) reveal the formation of nanosize and crystalline $CaWO_4:Dy^{3+}$. Dependence of energy transfer rate from WO_4^{2-} to the activator (Dy^{3+}) is observed from the photoluminescence studies. An enhancement of energy transfer efficiency from 36% to 90% is observed after annealing the as-prepared samples at 800 °C. The exchange type energy transfer mechanism is observed to be dominant in as-prepared samples while the electric dipole-dipole interaction is dominant in annealed samples. Variation in energy transfer rate from the host to Dy^{3+} activator ions leads to the tuning of color emission from this nanophosphor. A near white light emission could be achieved with 6 at.% Dy^{3+} doped $CaWO_4$ annealed at 800 °C with $x = 0.310$ and $y = 0.327$.

Keywords Luminescence · Energy transfer · Color tunable · White light emission

Introduction

Solid state lighting has gained a tremendous attention in the past decade due to their high luminous efficiency, low energy consumption, good reliability and longer lifetime compared to other incandescent and fluorescent light sources [1–4]. There are many ways of achieving white light among which phosphor-converted white LEDs have attracted many researchers due to their high efficiency and low cost [5, 6]. Theoretically, the white light is produced by mixing diodes emitting blue, green and red. However, there are certain issues/challenges in this approach: (i) difference in driving voltages of diode to diode and different light intensities of individual LED, (ii) Multiple chips LED is subject to significant changes in color with temperature, (iii) different operating lifetime of different LEDs. Generally, the production of white light is adopted by direct combination of a blue LED chip and yellow phosphor, e.g. InGaN blue LED combined yttrium aluminum garnet ($Y_3Al_5O_{12}:Ce^{3+}$), however, it has poor color rendering index due to insufficient red component [1, 7]. On the other hand, a combination of UV LED with ZnCdS:Ag (red), ZnS:Cu,Al (green) and ZnS:Ag (blue) phosphors leads to very low luminescent efficiency due to the strong reabsorption of the blue light by the red and green phosphors [8, 9]. Therefore, many researches have lately focused on the development of single phase white light emitting phosphors for a better outcome such as $Sr_2MgSi_2O_7:Dy^{3+}$; $CaAl_2O_4:Dy^{3+}$, $YPVO_4:Dy^{3+}/Sm^{3+}$, $CaZr_4(PO_4)_6:Dy^{3+}$, etc. are some of the examples of long lasting white light emitting phosphors [1, 10–13].

Metal tungstate such as AWO_4 (A = Ca, Cd, Zn) being a self-activated luminescence material related to its tetrahedral WO_4 groups with broad intense absorption band is a promising material in many applications [14–18]. Among these, $CaWO_4$ shows broad blue emission band under UV excitation due to the presence of WO_4^{2-} groups associated with the charge transfer from the $2p$ state of oxygen to empty $5d$ state of tungsten atom. According to molecular orbital theory, the bands in the excitation and emission spectra can be attributed to the transitions from the $^1A_1$ ground state to the high vibration level of $^1B(^1T_2)$ and from the low vibration level of

✉ N. Shanta Singh
ssnaorem@nagalanduniversity.ac.in

[1] Department of Physics, Nagaland University, Lumami, Nagaland 798627, India

$^1B(^1T_2)$ to the $^1A_1$ ground state within the WO_4^{2-} ions [19, 20]. On the other hand, doping with various rare earth ions such as Eu^{3+}, Sm^{3+}, Dy^{3+}, Tb^{3+} etc. in appropriate host materials have always proved to be the most convenient way to enhance the luminescence property [21, 22]. Rare earth ions doped with $CaWO_4$ phosphors are also widely studied due to the occurrence of strong energy transfer (ET) to rare earth ions from broad absorption band originated from WO_4^{2-} which leads to high luminescent efficiency [3, 23–27]. Upon UV excitation, Dy^{3+} exhibits blue and yellow emission corresponding to $^4F_{9/2} \rightarrow {}^6H_{15/2}$ and $^4F_{9/2} \rightarrow {}^6H_{13/2}$ transitions at wavelengths (450–500) nm and (550–600) nm. There are reports on the tuning of emission color by doping Dy^{3+} into various host material due to their high energy transfer efficiency [1, 3, 24, 28]. Recently, luminescence studies on $CaWO_4$ doped with Dy^{3+} prepared via various techniques are reported, but only a few have reported on achieving high quantum efficiency and realization of white light in the visible region [25, 29–32]. So far there are limited reports on luminescence studies of singly doped $CaWO_4$:xDy^{3+} synthesized via hydrothermal route.

In this paper, we report the investigation on photoluminescence and energy transfer mechanism in Dy^{3+} doped $CaWO_4$ nanophosphors prepared by hydrothermal method [33]. From the investigation, it has revealed the dominant dipole-dipole mechanism of energy transfer from WO_4^{2-} to the excited states of Dy^{3+} ions. It is also further established the enhancement in the energy transfer efficiency with post heat treatment of the samples. On subsequent doping of Dy^{3+} into $CaWO_4$, there is a remarkable tuning of emission color due to the controlled energy transfer from WO_4^{2-} to Dy^{3+} ions which further leads to the emission of near white light emission.

Experimental

Synthesis

All the samples were synthesized using the hydrothermal technique. The starting materials: calcium nitrate tetrahydrate ($Ca(NO_3)_2{\cdot}4H_2O$, ≥ 99%), sodium tungstate dihydrate ($Na_2WO_4{\cdot}2H_2O$, ≥ 99%) and polyvinylpyrrolidone (PVP-40,000) were purchased from Sigma-Aldrich and dysprosium nitrate pentahydrate ($Dy(NO_3)_3{\cdot}5H_2O$, 99.9%) was purchased from Alfa Aesar. All the chemicals were used without any further purification. Typically, to synthesize $CaWO_4$ doped with Dy^{3+} (3 at.%), 500 mg of $Ca(NO_3)_2{\cdot}4H_2O$ and 29 mg of $Dy(NO_3)_3{\cdot}5H_2O$ were dissolved in 20 mL de-ionized water. To this, 5 mL polyvinylpyrrolidone (PVP) solution (5%) was added and stirred well. Later, 720 mg of $Na_2WO_4{\cdot}2H_2O$ was added and stirred until the whole solution gets fully dissolved. The final solution was maintained at pH = 6 using NaOH. Then the entire solution was transferred to a Teflon-lined stainless steel autoclave and heated at 180 °C for 15 h. The white precipitates so formed were collected and washed with de-ionized water and ethanol several times. The precipitates were dried at 50 °C overnight in air. Remaining samples were prepared by following the same procedure. All the as-prepared samples were annealed at 800 °C for 6 h in air. A schematic representation of the synthesis process is shown in Fig. 1.

Characterization

The structural characterization was carried out using Bruker, D8 Advance X-ray diffractometer. FT-IR spectroscopy studies were carried out using Shimadzu (model 8400S). Transmission electron microscopy (TEM) images were recorded using JEOL 2000FX. The steady state luminescence and decay

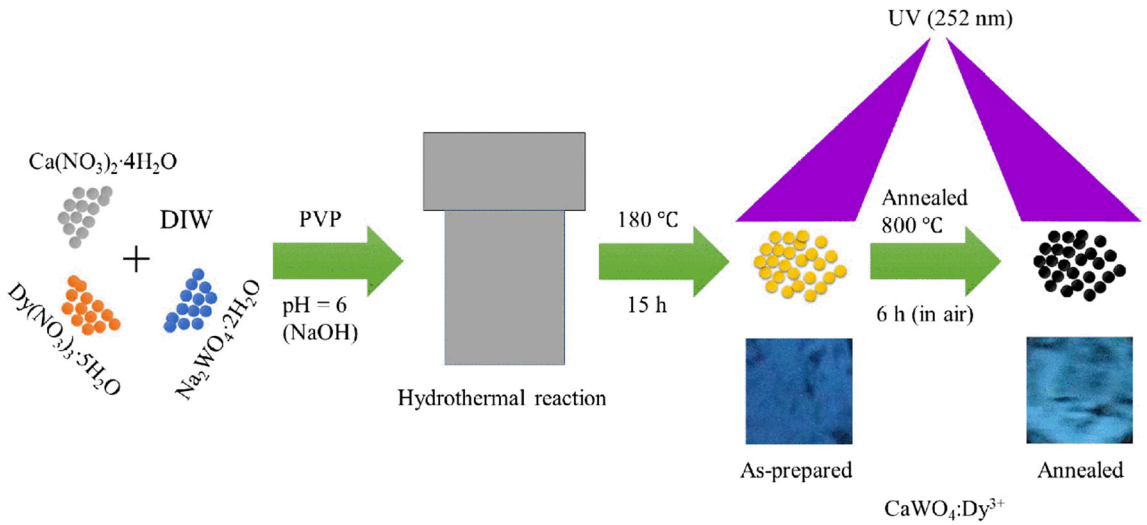

Fig. 1 A schematic representation of the synthesis of $CaWO_4$:Dy^{3+}

lifetime were measured with Horiba make FluoroMax-4CP Spectrofluorometer equipped with 150 W xenon lamp and 25 W μsec flash lamp as excitation sources.

Results and Discussion

XRD, FTIR and TEM Studies

The XRD patterns of as-prepared and 800 °C annealed bare $CaWO_4$ sample are shown in Fig. 2a. Figure 2b shows the XRD patterns of as prepared $CaWO_4$ doped Dy^{3+} (1, 5 and 7 at.%) samples. From the patterns, the observed diffraction peaks are corresponding to the tetragonal phase with the scheelite structure of $CaWO_4$ (JCPDS# 41–1431) with space group I41/a. No additional peaks were detected, suggesting the lattice site substitution of Ca^{2+} sites by Dy^{3+} ions. This possibility of lattice substitution may be understood from the viewpoint of nearly equal ionic radii of Ca^{2+} ($r = 1.12$ Å) and Dy^{3+} ($r = 1.03$ Å) for the system of CN = 8 in spite of their charge difference. From Scherrer relation [34], $d = k\lambda/\beta\mathrm{Cos}\theta$, where d is the average crystallite size, λ is the X-ray wavelength, θ is the diffraction angle and β is the full-width half maximum of the observed peaks, the average crystallite size is found to be ~ 12–20 nm. Figure 2c illustrates the XRD patterns of $CaWO_4$ doped Dy^{3+} (0, 1, 5 and 7 at.%) samples annealed at 800 °C. The patterns show more defined and sharper due to more crystallinity after heat treatment and the average crystallite size is found to be 16–24 nm.

Figure 3 depicts the FTIR spectra of 1 at.% Dy^{3+} doped $CaWO_4$ as-prepared sample. The band at 3381 cm^{-1} is assigned to the stretching vibration of O-H groups which corresponds to the water molecules physically absorbed on the surface of the sample. A small absorption peak at 2964 cm^{-1} is due to the asymmetric CH_2 stretching vibration [35]. The peaks at 1664 and 1290 cm^{-1} are the characteristic vibrations of C=O and C-N of PVP [36]. The band at 1456 cm^{-1} arises from the N-O vibration as a contribution from the remains of NO_3^- starting materials. The two absorption bands at 852 and 439 cm^{-1} belongs to the O-W-O stretching and W-O bending vibrations of WO_4 tetrahedron [26].

The structure and morphology of the synthesized nanoparticles were studied by TEM. As shown in Fig. 4a the particles are nearly spherical in shape. The average grain size of the nanoparticles so obtained from TEM ranges between 30 and 40 nm which is somewhat larger than that calculated from XRD peaks due to the agglomeration of the nanoparticles. Size distribution plot also reveals with a maximum number of particles in the range between 30 and 40 nm (Fig. 4d). The high-resolution TEM image of $CaWO_4$ is shown in Fig. 4b. The inset image shows the magnified image of the interplanar spacing of ~ 3.2 Å between the parallel planes corresponding to (112) planes. The selected area electron diffraction image in Fig. 4c shows the crystalline nature of $CaWO_4$ nanoparticles.

Photoluminescence (PL) Studies

Excitation spectra of as-prepared (ASP) samples of $CaWO_4$:xDy^{3+} ($x = 0$, 1, 3, 5, 6, 7 and 8 at.%) are displayed in Fig. 5a. Emission wavelength was monitored at 415 nm for bare $CaWO_4$ and 573 nm for all the Dy^{3+} doped $CaWO_4$ samples. All the spectra show a broad absorption band at around 255 nm in the range of 225–285 nm This band is attributed to the charge-transfer (CT) transition, $^1A_1 \rightarrow {}^1T_1$ originated from oxygen ligand 2p orbital to the empty central tungsten 5d orbital in the WO_4^{2-} complex. While the Dy – O CT band

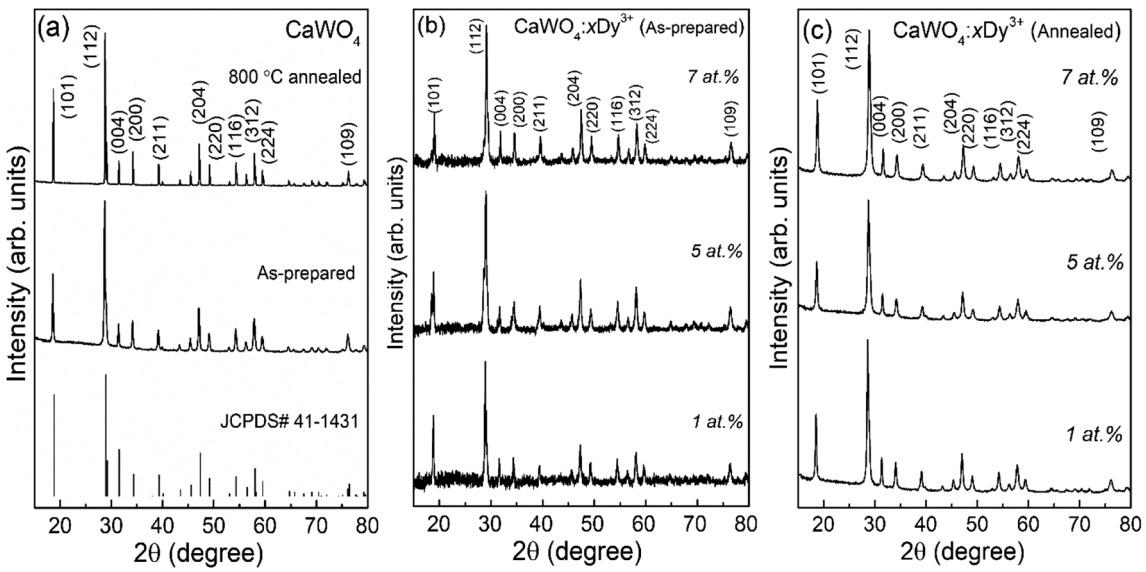

Fig. 2 XRD patterns of (**a**) bare $CaWO_4$, (**b**) as-prepared and (**c**) 800 °C annealed $CaWO_4$:Dy^{3+} samples

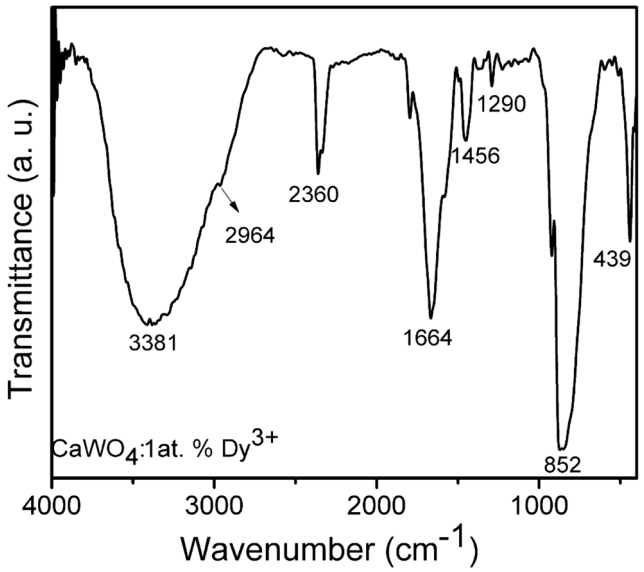

Fig. 3 FTIR spectra of 1 at.% Dy^{3+} doped $CaWO_4$ as-prepared sample

[37] is not observed distinctly, this may be due to the overlapped absorption region with W – O CT band. Similarly, annealed samples also show the presence of CT band in all the samples (Fig. 5b). The presence of these CT bands indicates the existence of energy transfer between WO_4^{2-} groups to the excited states of Dy^{3+} ions. In addition to the broad peak, many sharp absorption peaks are also observed in all the Dy^{3+} doped samples in the longer wavelength range. These peaks arise from the electronic transitions within *f*-shell of Dy^{3+} which correspond to $^6H_{15/2} \rightarrow {}^6P_{3/2}$ (325 nm), $^6H_{15/2} \rightarrow {}^6P_{7/2}$ (352 nm), $^6H_{15/2} \rightarrow {}^4I_{11/2}$ (366 nm), $^6H_{15/2} \rightarrow {}^4M_{19/2} + {}^4M_{21/2}$ (387 nm) and $^6H_{15/2} \rightarrow {}^4G_{11/2}$ (449/453 nm) [38, 39]. It can be noted that there is an enhancement in the *f-f* transitions absorption peaks after annealing the samples compared to as-prepared samples as shown in Fig. 6 (discussed later).

Figure 7 shows the emission spectra of (a) as-prepared and (b) 800 °C annealed Dy^{3+} doped $CaWO_4$ nanocrystals under 252 nm excitation. All the samples demonstrate the presence of a broad blue emission band ranging from 320 to 560 nm

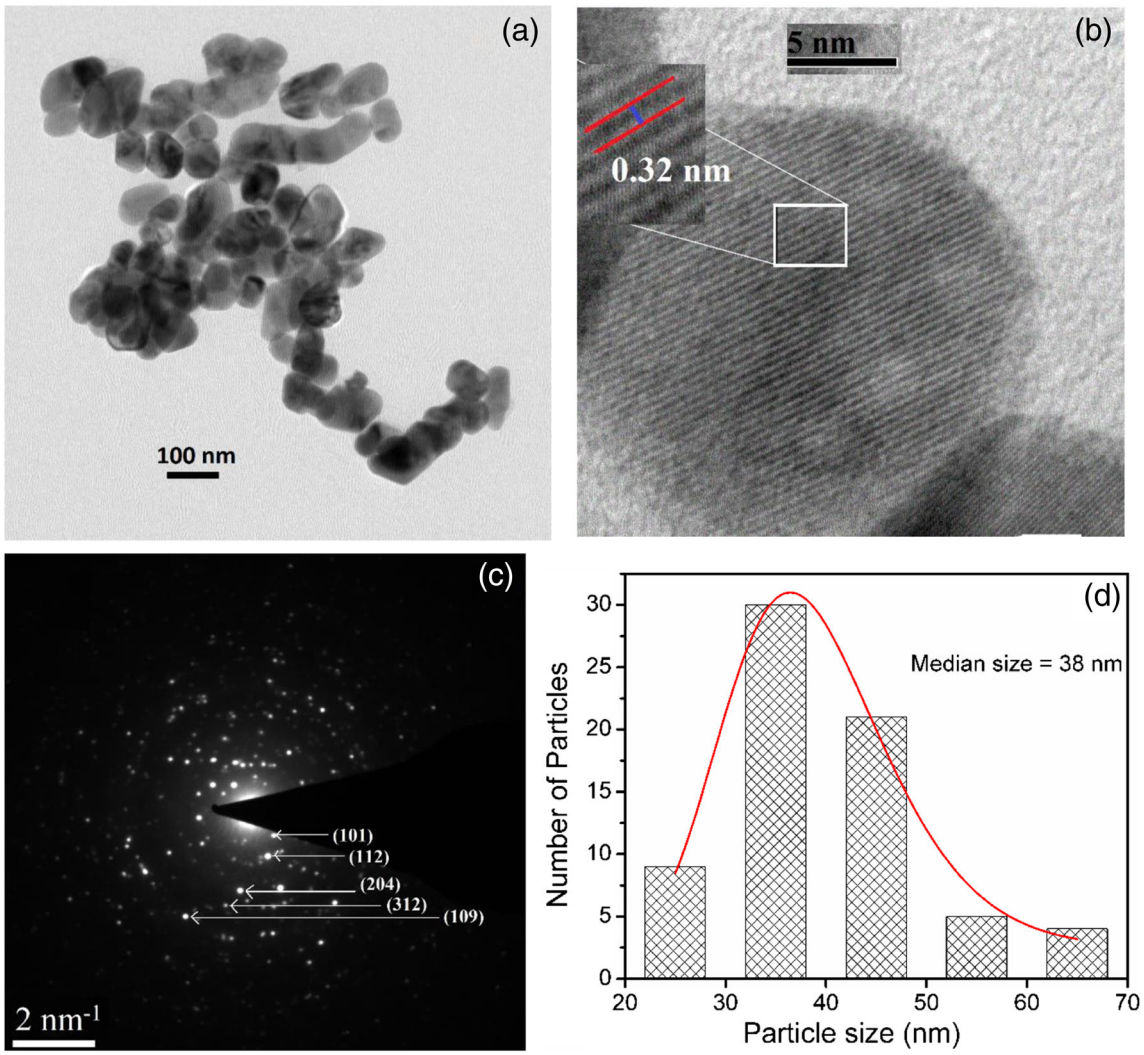

Fig. 4 **a** TEM image **b** HRTEM image and **c** SAED pattern and **d** size distribution of $CaWO_4$:Dy^{3+} (3 at.%) nanophosphor

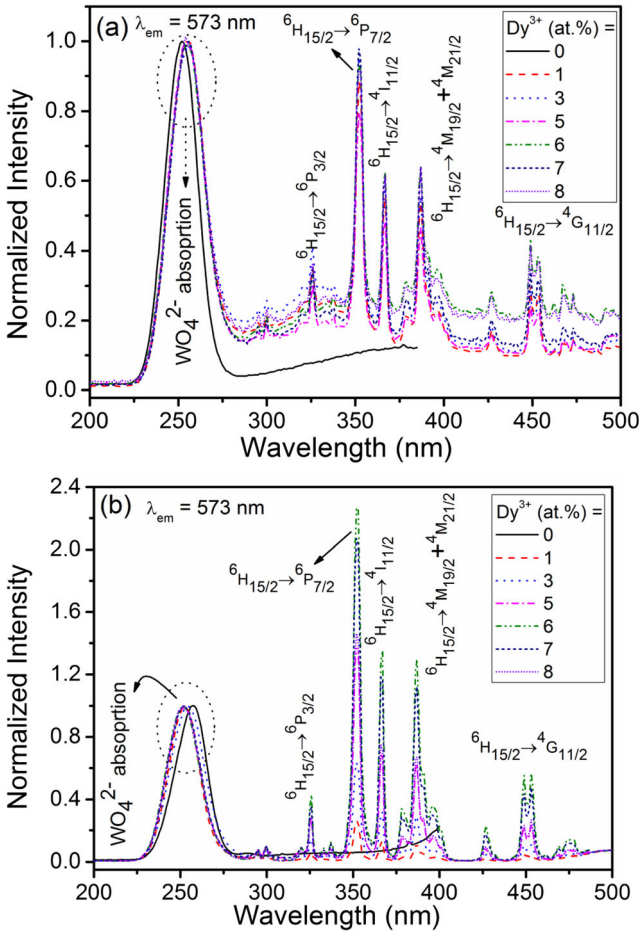

Fig. 5 Normalized (at WO_4^{2-} absoprtion) PL excitation spectra of (**a**) as-prepared and (**b**) 800 °C annealed $CaWO_4$:xDy^{3+} ($x = 0$, 1, 3, 5, 6, 7 and 8 at.%) samples, monitored at 573 nm emission wavelength

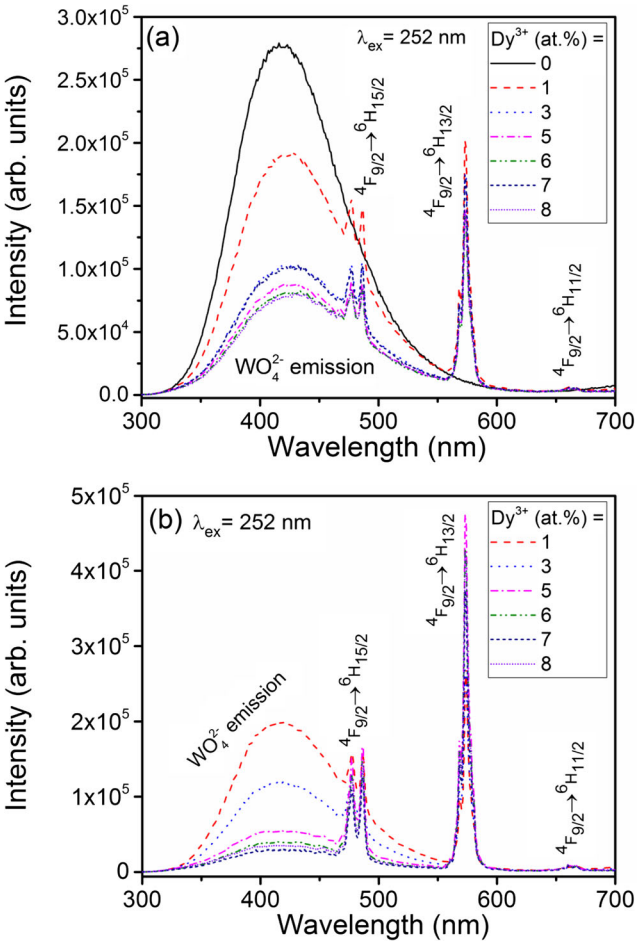

Fig. 7 PL emission spectra of (**a**) as-prepared and (**b**) 800 °C annealed $CaWO_4$:xDy^{3+} ($x = 0$, 1, 3, 5, 6, 7 and 8 at.%) samples at under 252 nm excitation

with maximum intensity centred at around 430 nm which is due to radiative transitions within the CT of WO_4^{2-} groups. Additionally, in both the cases emission peaks related to the *f-f*

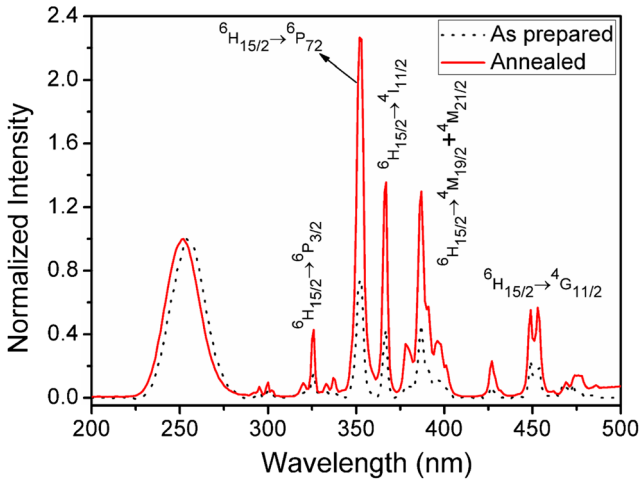

Fig. 6 Comparative PL excitation spectra of as-prepared and 800 °C annealed $CaWO_4$:Dy^{3+} (6 at.%) nanophosphors monitored at 573 nm emission wavelength (normalized at WO_4^{2-} absorption)

transitions are also observed. These transitions are located at 477/486, 573 and 661 nm corresponding to $^4F_{9/2} \rightarrow {}^6H_{15/2}$, $^4F_{9/2} \rightarrow {}^6H_{13/2}$ and $^4F_{9/2} \rightarrow {}^6H_{11/2}$ transitions of Dy^{3+} ions [1, 38]. The spectra in Fig. 7 show the decrease in the broad WO_4^{2-} emission band with the increment in the Dy^{3+} concentration in $CaWO_4$:xDy^{3+} nanoparticles. This indicates the transfer of energy from WO_4^{2-} group to Dy^{3+} ions. Emission peaks at 477 and 486 nm are associated with parity allowed magnetic dipole transitions. While the peak at 573 ($^4F_{9/2} \rightarrow {}^6H_{13/2}$) nm is attributed to the electric dipole transition of Dy^{3+} which is hypersensitive to the surrounding of the Dy^{3+} ions. In all the cases, electric dipole transitions are dominant over the magnetic dipole transitions. This phenomenon can be understood from the symmetry point of view of Ca – O octahedral. When the Dy^{3+} occupies the Ca^{2+} site in the host lattice $CaWO_4$ in the scheelite structure having space group C_{4h} with S_4 point symmetry with no inversion center leads to the hypersensitive electric dipole transition. Though there is charge difference between Ca^{2+} and Dy^{3+}, near similar ionic radii of (in CN 8) Ca^{2+} ($r = 1.12$ Å) and Dy^{3+} ($r = 1.03$ Å), substitution of Ca^{2+} lattice sites by Dy^{3+} occurred. During the

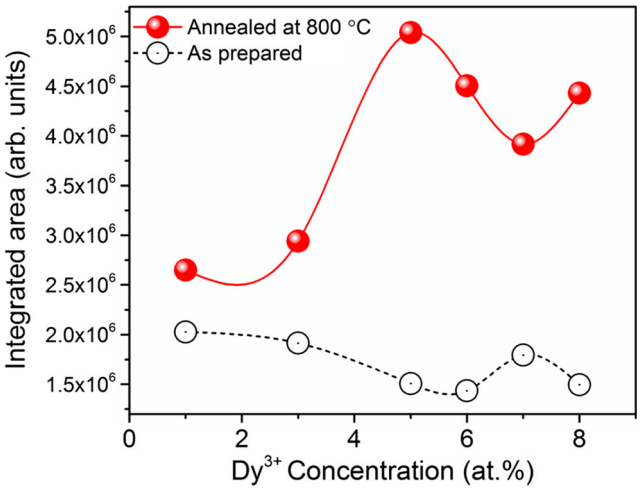

Fig. 8 Comparative emission intensity (573 nm emission) of as-prepared and 800 °C annealed $CaWO_4$:xDy^{3+} (x = 1, 3, 5, 6, 7 and 8 at.%) nanophosphors under 252 nm excitation

substitution, 2 lattice sites of Ca^{2+} are replaced by 2 Dy^{3+} ions with the creation of a vacancy site at Ca^{2+} site for the requirement of charge compensation (i.e., $3Ca^{2+} \rightarrow 2Dy^{3+}+\square$ (vacancy)) [32, 40]. This further adds to more asymmetric environment around Dy^{3+} surroundings. Thus, it might again have led to more deviation from actual S_4 site symmetry [41]. A careful comparison of as-prepared and annealed samples reveals the enhancement of *f-f* transitions emission with the substantial reduction in the luminescence intensity of the broadband emission due to WO_4^{2-} groups after the samples annealed 800 °C. This may be understood due to the enhancement in the energy transfer processes from WO_4^{2-} groups to activators in the annealed samples. On the other hand, upon annealing occupation of Ca^{2+} lattice by Dy^{3+} ions increase thereby enhances the occurrence of resonance energy transfer. This may also be correlated to the increase asymmetric ratio which is defined by the ratio of emission intensity due to the electric dipole transition ($^4F_{9/2} \rightarrow {}^6H_{13/2}$) to that of the magnetic dipole transition ($^4F_{9/2} \rightarrow {}^6H_{15/2}$). On the other hand, annealing helps to the removal of -OH groups and organic capping agents (polyvinylpyrrolidone) adsorbed on the particle surface which can act as quenching sites for non-radiative pathways. This removal can reduce such unwanted processes. Thus, luminescence is enhanced after annealing (Fig. 8).

Energy Transfer Mechanism

The energy transfer efficiency (η_T) from host to activator in ASP and 800 °C annealed $CaWO_4$:Dy^{3+} upon 252 nm excitation can be calculated by the following equation [7],

$$\eta_T = 1 - I_S/I_{S0} \quad (1)$$

where η_T is the energy transfer efficiency, I_S and I_{S0} are the luminescence intensities of the host in the presence and absence of an activator (Dy^{3+}) respectively. Figure 9 shows the plot of the energy transfer efficiency and the concentration of the Dy^{3+} ions for both the ASP and 800 °C annealed $CaWO_4$:xDy^{3+} (x = 0, 1, 3, 5, 6, 7 and 8 at. %). In both the cases, the energy transfer efficiencies increase with the increase of Dy^{3+} ion concentration. This could be due to the increase in the availability of randomly distributed Dy^{3+} ions in the host matrix ($CaWO_4$) with the increase of concentration. It is also observed that the efficiency of energy transfer from the host to the activator for annealed sample is much higher as compared to that of ASP sample. Energy transfer efficiency could be achieved up to a maximum value of 36% and 90% respectively, in ASP and 800 °C annealed samples.

The energy transfer process or concentration quenching mechanism can be defined as of two different interactions: exchange and multipolar interactions [25, 42–44]. Based on Dexter's energy transfer theory and Reisfeld's approximation, the following relationship can be used to investigate the mode of interaction(s) [45],

$$I/x \sim \left(\beta x^{\theta/3}\right)^{-1} \text{ or } log(I/x) = c - (\theta/3)\log x \quad (2)$$

where I is the emission intensity, x is the concentration of Dy^{3+} ions, θ represents the interaction types, β and c are constants for a particular host under the same excitation parameters. The values of θ are 3, 6, 8, and 10, corresponding to the exchange coupling, electric dipole-dipole, dipole-quadrupole and quadrupole-quadrupole interactions, respectively. The relation between $log(I/x)$ and $logx$ along with linearly fitted plots are shown in Fig. 10. From the figure, it is observed that both ASP and 800 °C annealed samples follow a linear relationship with slopes −1.21 and − 2.09 respectively. Therefore, θ values were calculated to be 3.63 and 6.27. So, it may be concluded that, in ASP samples

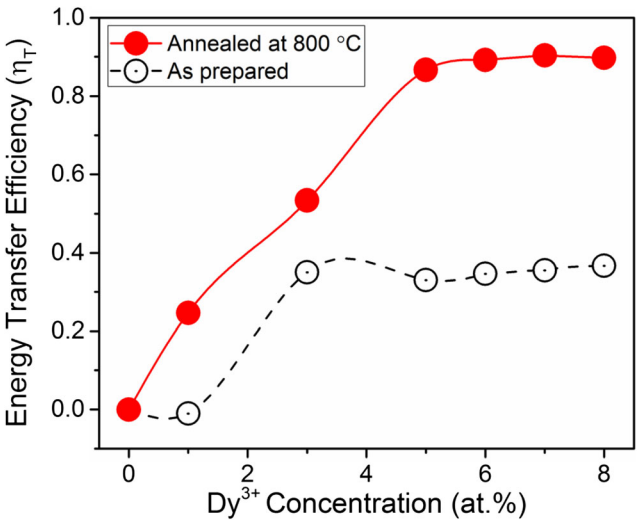

Fig. 9 Dependence of energy transfer efficiency (η_T) on doped Dy^{3+} concentration in as-prepared and 800 °C annealed $CaWO_4$:xDy^{3+} (x = 0, 1, 3, 5, 6, 7 and 8 at.%) nanophosphors under 252 nm excitation

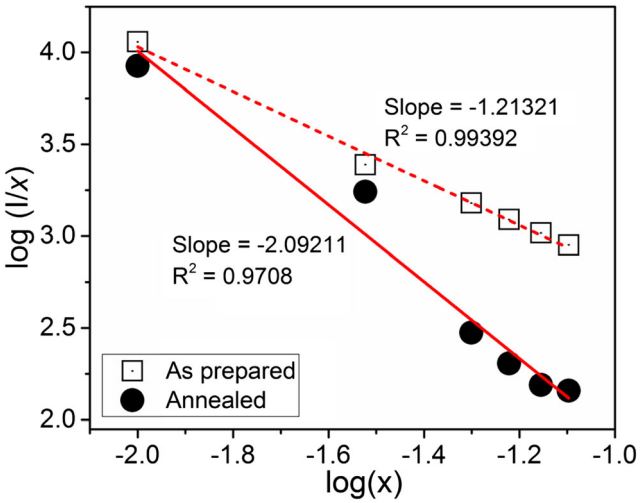

Fig. 10 Plot of $log(I/x)$ versus $logx$ for $^4F_{9/2} \rightarrow {}^6H_{13/2}$ transition of x at.% Dy^{3+} ions in $CaWO_4$ nanophosphors

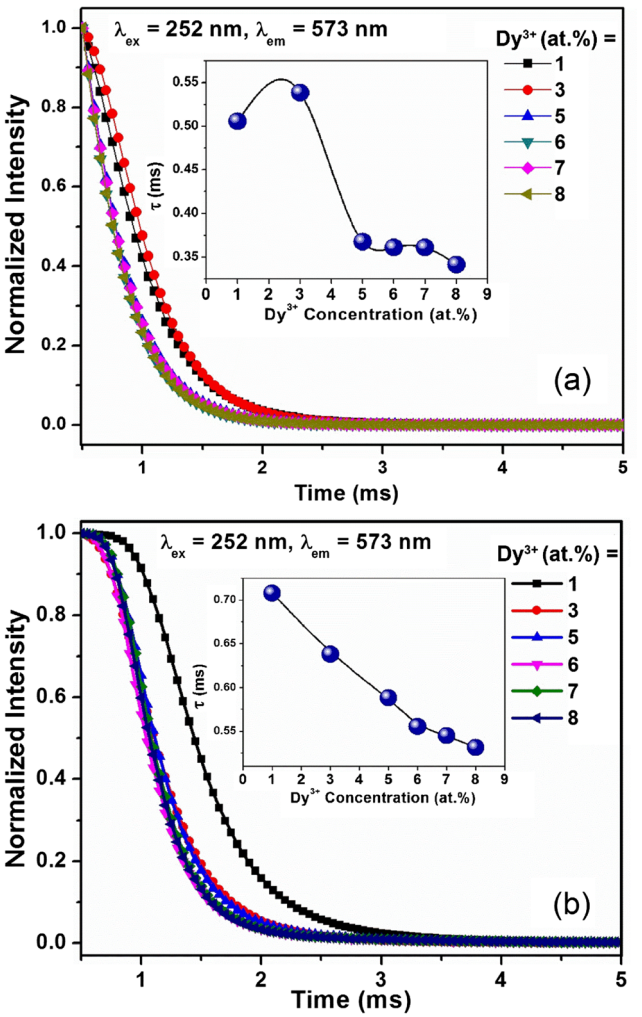

Fig. 11 PL decay curves of (**a**) as-prepared and (**b**) 800 °C annealed $CaWO_4$:xDy^{3+} (x = 1, 3, 5, 6, 7 and 8 at.%) nanophosphors monitored at 252 nm excitation and 573 nm emission

Table 1 Luminescence decay lifetime of the as-prepared and 800 °C annealed $CaWO_4$:xDy^{3+} (x = 1, 3, 5, 6, 7 and 8 at.%) nanophosphors under 252 nm excitation

Dy^{3+} concentration (at.%)	Decay lifetime (ms)	
	ASP	Annealed
1	0.506	0.708
3	0.539	0.638
5	0.368	0.588
6	0.339	0.555
7	0.361	0.545
8	0.342	0.531

exchange coupling (as $\theta = 3.63$ which is closer to theoretical value 3 than 6) is mainly responsible for energy transfer mechanism in Dy^{3+} doped $CaWO_4$ as-prepared samples. However, in 800 °C annealed samples the dominant mechanism for the energy transfer to Dy^{3+} ions in $CaWO_4$ nanophosphors is due to the electric dipole-dipole interaction (as $\theta = 6.27$ which is very close to theoretical value 6 of dipole-dipole interaction).

Decay Lifetime Study

The PL decay curves of the $^4F_{9/2} \rightarrow {}^6H_{13/2}$ transition monitored at 573 nm emission for the ASP and 800 °C annealed $CaWO_4$:xDy^{3+} (x = 1, 3, 5, 6, 7 and 8 at. %) nanophosphors under excitation at 252 nm wavelength are displayed in Fig. 11. The decay curves can be well fitted by a mono-exponential decay equation as given by the expression [38, 46],

$$I(t) = I_0 \exp(-t/\tau) \quad (3)$$

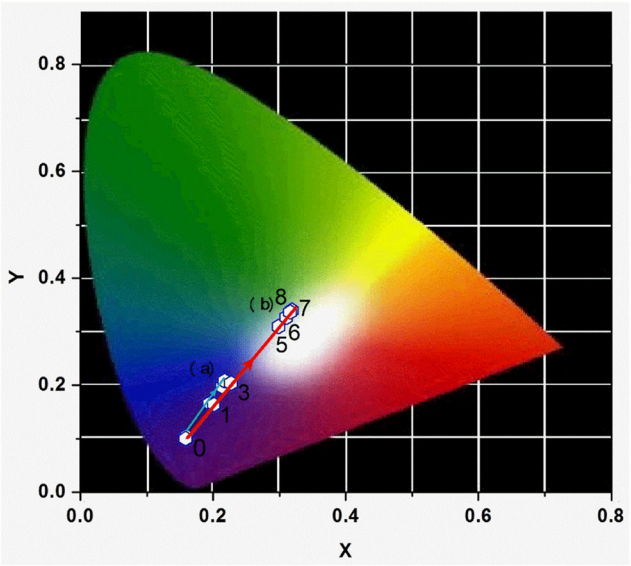

Fig. 12 CIE chromaticity diagram of the as-prepared and 800 °C annealed $CaWO_4$:xDy^{3+} (x = 0, 1, 3, 5, 6, 7 and 8 at.%) nanophosphors excited at 252 nm

Table 2 CIE colour coordinates of the as-prepared and 800 °C annealed $CaWO_4$:xDy^{3+} ($x = 0$, 1, 3, 5, 6, 7 and 8 at.%) nanophosphors under 252 nm excitation

Dy^{3+} concentration (at.%)	CIE coordinates (*x, y*)	
	ASP	Annealed
0	(0.160, 0.105)	(0.159, 0.100)
1	(0.194, 0.166)	(0.201, 0.164)
3	(0.214, 0.199)	(0.227, 0.204)
5	(0.214, 0.200)	(0.299, 0.310)
6	(0.215, 0.202)	(0.310, 0.327)
7	(0.213, 0.197)	(0.319, 0.340)
8	(0.217, 0.208)	(0.316, 0.337)

where I is the luminescence intensity at t, I_0 is the initial intensity at $t = 0$, and τ is the decay lifetime. The calculated lifetime values of the ASP and annealed $CaWO_4$:xDy^{3+} are given in Table 1. It is found that in both the cases the decay lifetime values decrease with the increase of Dy^{3+} concentration. This may be due to the increase in the non-radiative decay rates. Such phenomena have been reported earlier by us [38].

CIE Chromaticity Study

The Commission Internationale d I'Eclairage (CIE) [47] chromaticity diagrams with positions of the respective chromaticity coordinates of the corresponding PL spectra of ASP and 800 °C annealed $CaWO_4$:xDy^{3+} ($x = 0$, 1, 3, 5, 6, 7 and 8 at.%) nanophosphors upon UV excitation at 252 nm are shown in Fig. 12. The calculated CIE coordinates (*x, y*) so obtained for both the ASP and annealed samples are also presented in Table 2. It is observed that the chromaticity coordinates of $CaWO_4$:xDy^{3+} vary with different Dy^{3+} ion concentrations. The blue line (a) and the red line (b) in Fig. 12, depicted the chromaticity coordinates of the ASP and 800 °C annealed $CaWO_4$:xDy^{3+} nanophosphors. Also, doping concentrations (at.%) are indicated in the figure for annealed samples. Upon 252 nm excitation the emission colors of all ASP samples are located at the blue region approaching towards white which is due to the decrease in the WO_4^{2-} emission contribution with the increase of Dy^{3+}. On the other hand, on annealing the samples at 800 °C, emission colors can be tuned from blue to yellowish green. Interestingly, near white light emission could be achieved with 6 at.% Dy^{3+} doped $CaWO_4$ nanoparticles annealed at 800 °C with $x = 0.310$ and $y = 0.327$. These tuning effects are possible due to the variation of energy transfer from the host to Dy^{3+} activator ions due to the combined admixture of WO_4^{2-} and Dy^{3+} emissions. As a result, by controlling the doping concentration of the activator ions and by annealing the sample, emission color can be tuned and white light can be produced.

Conclusions

We have successfully synthesized $CaWO_4$:xDy^{3+} (0, 1, 3, 5, 6, 7 and 8 at. %) nanophosphors via hydrothermal route. From the photoluminescence investigation, it is established that the rate of energy transfer from WO_4^{2-} to the activator (Dy^{3+}) depends on the concentration and annealing. It is further observed that the energy transfer efficiency is increased from 36% to 90% after annealing the as-prepared samples at 800 °C. The energy transfer mechanism from host to activators is dominated by exchange type in as-prepared samples, while electric dipole-dipole interaction mechanism is dominant in annealed samples. It is also observed that the variation in energy transfer rates from the host to Dy^{3+} activator ions leads to the tuning of color emission from this nanophosphor. A near white light emission could be achieved with 6 at.% Dy^{3+} doped $CaWO_4$ nanoparticles annealed at 800 °C with $x = 0.310$ and $y = 0.327$.

Acknowledgments Authors thank Science & Engineering Research Board (DST), New Delhi, for financial support (EMR Project No. EMR/2014/001211). T. Yaba thanks UGC, New Delhi for financial support. Authors thank SAIF, NEHU, Shillong for TEM facility.

References

1. Singh NS, Sahu NK, Bahadur D (2014) Multicolor tuning and white light emission from lanthanide doped YPVO4 nanorods: energy transfer studies. J Mater Chem C 2:548–555
2. Pradal N, Chadeyron G, Potdevin A, Deschamps Y, Mahiou R (2013) Elaboration and optimization of Ce-doped $Y_3Al_5O_{12}$ nanopowder dispersions. J Eur Ceram Soc 33:1935–1945
3. Khanna A, Dutta PS (2012) $CaWO_4$: Eu^{3+}, Dy^{3+}, Tb^{3+} phosphor crystals for solid-state lighting applications. ECS Trans 41(37):39–48
4. Varun S, Kalra M, Gandhi M (2015) White light emission through downconversion of terbium and europium doped CeF_3 nanophosphors. J Fluoresc 25(5):1501–1505
5. Smet PF, Korthout K, Haecke JEV, Poelman D (2007) Using rare earth doped thiosilicate phosphors in white light emitting LEDs: towards low colour temperature and high colour rendering. Mater Sci Eng B 146:264–268
6. Kim JS, Jeon PE, Choi JC, Park HL, Muo SI, Kim GC (2004) Warm-white-light emitting diode utilizing a single-phase full-color $Ba_3MgSi_2O_8$:Eu^{2+}, Mn^{2+} phosphor. Appl Phys Lett 84(15):2931–2933
7. Wangkhem R, Yaba T, Singh NS, Ningthoujam RS (2018) Red emission enhancement from $CaMoO_4$:Eu^{3+} by co-doping of Bi^{3+} for near UV/blue LED pumped white pcLEDs: energy transfer studies. J Appl Phys 123:124303
8. Sato Y, Takahashi N, Sato S (1996) Full-color fluorescent display devices using a near-UV light-emitting diode. Jpn J Appl Phys 35:838–839
9. Shang M, Li C, Lin J (2014) How to produce white light in a single-phase host? Chem Soc Rev 43:1372–1386

10. Liu B, Kong L, Shi C (2007) White-light long-lasting phosphor $Sr_2MgSi_2O_7:Dy^{3+}$. J Lumin 122-123:121–124
11. Liu B, Shi C, Qi Z (2005) Potential white-light long-lasting phosphor: Dy^{3+} −doped aluminate. Appl Phys Lett 86:191111
12. Ye S, Xiao F, Pan YX, Ma YY, Zhang QY (2010) Phosphors in phosphor-converted white light-emitting diodes: recent advances in materials, techniques and properties. Mater Sci Eng R 71:1–34
13. Nair GB, Dhoble SJ (2017) White light emitting $MZr_4(PO_4)_6:Dy^{3+}$ (M = ca, Sr, Ba) phosphors for WLEDs. J Fluoresc 27(2):575–585
14. Tanaka K, Miyajima T, Shivai N, Zhang Q, Nakata R (1995) Laser photochemical ablation of $CdWO_4$ studied with the time-of-flight mass spectrometric technique. J Appl Phys 77(12):6581–6587
15. Wang H, Medina FD, Zhou YD, Zhang QN (1992) Temperature dependence of the polarized Raman spectra of ZnWO4 single crystals. Phys Rev B 45(18):10356–10362
16. Basu S, Naidu BS, Viswanadh B, Sudarson V, Jha SN, Bhattacharyya D, Vatsa RK (2014) Nature of WO_4 tetrahedra in blue light emitting $CaWO_4$ probed through the EXAFS technique. RSC Adv 4:15606–15612
17. Grasser R, Scharmann A, Strack KR (1982) On the intrinsic nature of the blue luminescence in $CaWO_4$. J Lumin 27:263–272
18. Mv S, Ciemniak C, Erb A, Fv F, Gütlein A, Lanfranchi J-C, Lepelmeier J, Münster A, Potzel W, Roth S, Strauss R, Thalhammer U, Wawoczny S, Willers M, Zöller A (2012) Influence of annealing on the optical and scintillation properties of $CaWO_4$ single crystals. Opt Mater 34:1843–1848
19. Kang F, Peng M (2014) A new study on the energy transfer in the color-tunable phosphor $CaWO_4$:bi. Dalton Trans 43:277–284
20. Treadaway MJ, Powell RC (1974) Luminescence of calcium tungstate crystals. J Chem Phys 61(10):4003–4011
21. Feldmann C, Justel T, Ronda CR, Schmidt PJ (2003) Inorganic luminescent materials: 100 years of research and application. Adv Funct Mater 13(7):511–516
22. Hoppe HA (2009) Recent developments in the field of inorganic phosphors. Angew Chem Int Ed 48:3572–3582
23. Treadaway MJ, Powell RC (1975) Energy transfer in samarium-doped calcium tungstate crystals. Phys Rev B 11(2):862–874
24. Su Y, Li L, Li G (2009) Generation of tunable wavelength lights in core-shell $CaWO_4$ microspheres via co-doping with Na^+ and ln^{3+} (Ln = Tb, Sm, Dy, Eu). J Mater Chem 19:2316–2322
25. Du P, Bharat LK, Guan XY, Yu JS (2015) Synthesis and luminescence properties of color-tunable Dy^{3+}-activated $CaWO_4$ phosphors. J Appl Phys 117:083112
26. Sharma KG, Singh NS, Devi YR, Singh NR, Singh SD (2013) Effects of annealing on luminescence of $CaWO_4:Eu^{3+}$ nanoparticles and its thermoluminescence study. J Alloys Compd 556:94–101
27. Liao J, Qiu B, Wen H, You W (2009) Photoluminescence green in microspheres of $CaWO_4:Tb^{3+}$ processed in conventional hydrothermal. Opt Mater 31:1513–1516
28. Singh LR, Ningthoujam RS, Singh NS, Singh SD (2009) Probing Dy^{3+} ions on the surface of nanocrystalline YVO_4: luminescence study. Opt Mater 32:286–292
29. Zhang Y, Gong W, Yu J, Pang H, Song Q, Ning G (2015) A new single-phase white-light-emitting $CaWO_4:Dy^{3+}$ phosphor: synthesis, luminescence and energy transfer. RSC Adv 5:62527–62533
30. Xie W, Liu G, Dong X, Wang J, Yu W (2016) Doping Eu^{3+}/Sm^{3+} into $CaWO_4:Tm^{3+}$, Dy^{3+} phosphors and their luminescent properties, tunable color and energy transfer. RSC Adv 6:26239–26246
31. Sharma KG, Singh NR (2013) Synthesis and luminescence properties of $CaMO_4:Dy^{3+}$ (M = W, Mo) nanoparticles prepared via an ethylene glycol route. New J Chem 37:2784–2791
32. Du C, Lang F, Su Y, Liu Z (2013) Low temperature nanocasting synthesis of lanthanide ions (ln = Tb, Eu, Dy) doped $CaWO_4$ mesoporous structure with efficiently luminescent properties. J Colloid Interface Sci 394:94–99
33. Byrappa K, Adschiri T (2007) Hydrothermal technology for nanotechnology. Prog Cryst Growth Charact Mater 53:117–166
34. Patterson AL (1939) The Scherrer formula for X-ray particle size determination. Phys Rev 56:978–982
35. Koczkur KM, Mourdikoudis S, Polavarapu L, Skrabalak SE (2015) Polyvinylpyrrolidone (PVP) in nanoparticle synthesis. Dalton Trans 44:17883–17905
36. Dhumale VA, Gangwar RK, Datar SS, Sharma RB (2012) Reversible aggregation control of polyvinylpyrrolidone capped gold nanoparticles as a function of Ph. Mater. Express 2(4):311–318
37. Omkaram I, Buddhudu S (2009) Photoluminescence properties of $MgAl_2O_4:Dy^{3+}$ powder phosphor. Opt Mater 32:8–11
38. Singh NS, Ningthoujam RS, Luwang MN, Singh SD, Vasta RK (2009) Luminescence, lifetime and quantum yield studies of $YVO_4:Ln^{3+}$ (Ln^{3+} = Dy^{3+}, Eu^{3+}) nanoparticles: concentration and annealing effects. Chem Phys Lett 480:237–242
39. Nayar R, Tamboli S, Sahu AK, Nayar V, Dhoble SJ (2017) Synthesis and luminescence characterization of $LaBO_3:Dy^{3+}$ phosphor for stress sensing application. J Fluoresc 27(1):251–261
40. Cavalcante LS, Longo VM, Sczancoski JC, Almeida MAP, Batista AA, Varela JA, Orlandi MO, Longo E, Li MS (2012) Electronic structure, growth mechanism and photoluminescence of $CaWO_4$ crystals. CrystEngComm 14:853–868
41. Hou Z, Li C, Yang J, Lian H, Yang P, Chai R, Chang Z, Lin J (2009) One-dimensional $CaWO_4$ and $CaWO_4:Tb^{3+}$ nanowires and nanotubes: electrospinning preparation and luminescent properties. J Mater Chem 19:2737–2746
42. Tian Y, Chen B, Tian B, Hua R, Sun J, Cheng L, Zhong H, Li X, Zhang J, Zheng Y, Yu T, Huang L, Meng Q (2011) Concentration-dependent luminescence and energy transfer of flower-like $Y_2(MoO_4)_3:Dy^{3+}$ phosphor. J Alloys Compd 509:6096–6101
43. Jiao M, Jia Y, Lu W, Lv W, Zhao Q, Shao B, You H (2014) $Sr_3GdNa(PO_4)_3F:Eu^{2+},Mn^{2+}$: a potential color tunable phosphor for white LEDs. J Mater Chem C 2:90–97
44. Zhang Q, Meng Q, Sun W (2013) The concentration dependence of luminescent properties for Eu^{3+} doped $CaWO_4$ micron spherical phosphors. Opt Mater 35:915–922
45. Dexter DL (1953) A theory of sensitized luminescence in solids. J Chem Phys 21:836–850
46. Blasse G, Grabmaier BC (1994) Luminescent Materials, 1st edn. Springer-Verlag, Berlin Heidelberg
47. Smith T, Guild J (1931–32) The C.I.E. colorimetric standards and their use. Trans. Opt. Soc 33:73–134